batteries

MDPI

Article

Comparative Study of Online Open Circuit Voltage Estimation Techniques for State of Charge Estimation of Lithium-Ion Batteries

Hicham Chaoui [1,*] and Sravanthi Mandalapu [2]

[1] Department of Electronics, Carleton University, 1125 Colonel By Drive, Ottawa, ON K1S 5B6, Canada
[2] Department of Electrical and Computer Engineering, Tennessee Technological University, 220 W. 10th Street, Cookeville, TN 38505, USA; smandalap42@students.tntech.edu
* Correspondence: hicham.chaoui@carleton.ca; Tel.: +1-613-520-2600 (ext. 7467); Fax: +1-613-520-5708

Academic Editor: Maciej Swierczynski
Received: 19 January 2017; Accepted: 29 March 2017; Published: 6 April 2017

Abstract: Online estimation techniques are extensively used to determine the parameters of various uncertain dynamic systems. In this paper, online estimation of the open-circuit voltage (*OCV*) of lithium-ion batteries is proposed by two different adaptive filtering methods (i.e., recursive least square, *RLS*, and least mean square, *LMS*), along with an adaptive observer. The proposed techniques use the battery's terminal voltage and current to estimate the *OCV*, which is correlated to the state of charge (*SOC*). Experimental results highlight the effectiveness of the proposed methods in online estimation at different charge/discharge conditions and temperatures. The comparative study illustrates the advantages and limitations of each online estimation method.

Keywords: lithium-ion batteries; least mean square (*LMS*); recursive least square (*RLS*); open-circuit voltage (*OCV*) estimation

1. Introduction

Lithium-ion batteries have a higher energy and power density with respect to other chemistries like nickel cadmium (NiCad), nickel metal hydride (NiMH), and lead–acid [1,2]. Additionally, lithium-ion batteries have numerous advantages, such as compact size, low weight, high capacity, rapid charge capability, long cycle life, wide temperature operation range, low rate of self-discharge, no outgassing of hydrogen, and no memory effects [3]. These batteries have been widely used in real-time applications such as consumer electronics, automotive, and power tools. For these applications, the estimation of the state of charge (*SOC*) plays a vital role in their performance, since an inaccurate *SOC* estimation would damage the battery and consequently reduce its lifetime and performance.

Traditional *SOC* estimation techniques are used because of their simplicity. A basic real-time *SOC* estimation is coulomb counting (also called ampere-hour counting method), which is an open-loop algorithm that uses the battery's entering and leaving currents and integrates them through time. This method has several flaws, such as the accumulation of current sensor errors and difficulty in determining the initial value of *SOC* [4]. Despite its flaws, it is preferred in real-time applications where high accuracy is not a requirement. The other method to estimate *SOC* uses open-circuit voltage (*OCV*), which is related to the charge status of the battery [5]. However, this statement is true only when the battery is in steady-state. Therefore, a hybrid estimation technique combines the coulomb counting and *OCV* methods. However, some applications need continuous operation and do not allow the battery to reach steady-state, which increases the need for online *SOC* estimation techniques.

Numerous advanced estimation techniques are proposed at the expense of higher computation due to complex design. A simple battery model is implemented in [6] with a sliding mode observer to compensate for modeling uncertainties. In [7], a reduced observer technique is proposed to estimate *SOC*. However, this estimation technique requires the knowledge of the battery's parameters, which leads to reduced accuracy with aging. This drawback has been overcome with the adaptive *SOC* estimation strategy in [8]. Particle filter (PF) is a sequential Monte Carlo method which uses the samples of random weights (particles) for the estimation probability distribution function of nonlinear systems [8]. The Kalman filter (KF) has been widely used for the estimation of *OCV* and other battery parameters which have a direct relationship with the *SOC* [9]; this filter is a recursive algorithm that estimates the internal dynamic states of a system. To consider the nonlinear behavior of *OCV*, an extended Kalman filter (EKF) and unscented Kalman filter (UKF) are proposed in [10]. The fundamental principle of EKF is to linearize the nonlinear functions by using an expansion of a first-order Taylor series. Certain statistical assumptions and local linearization of state equations are the drawbacks of this well-known filter [11]. In [12], a different definition of *SOC* is proposed for a pack of batteries connected in series by finding out the voltage at the battery's terminals. Then, *SOC* is estimated using EKF, which yields nearly half of the error compared to the two time constant (TTC) method. In [13], a comparison between EKF and square root unscented Kalman filter (SR-UKF) shows better performance of SR-UKF with respect to EKF. Another *SOC* estimation technique with adaptive extended Kalman filter (AEKF) and wavelet transform matrix (WTM) is proposed in [14] to avoid the electromagnetic noise created in the measurement of voltage and current in electric vehicles (EVs). In addition, a fractional order Kalman Filter approach is introduced in [15] to estimate *SOC* based on fractional order model. An H_∞ observer is applied to estimate the *SOC* of a battery depending on the equivalent circuit of the linear state space model used as an inspection robot on a power transmission line [16].

Moreover, fuzzy logic and neural networks are widely used for robust approximation of systems subjected to uncertainties [17]. Various strategies are applied to estimate the *SOC* and yield acceptable results [18,19]. Although neural networks provide satisfactory performance, they fail to incorporate any human expertise already acquired about the dynamics of the system at hand. This shortcoming has been overcome by adopting different models of fuzzy neural networks in [20,21], but at the cost of higher computation.

This paper presents a comparative study of different online *OCV* estimation techniques for lithium-ion batteries. Here, two adaptive filtering methods— namely, least mean square (*LMS*) and recursive least square (*RLS*)—are designed and implemented. Moreover, an adaptive observer is also implemented for comparison purposes. It is important to note that all compared estimation strategies do not require any prior knowledge of the battery's parameters. Numerous comparative studies have been presented for *SOC* estimation [22–31]. While few studies investigate the impact of different battery circuit models on the *SOC* estimation [22–24], others focus on the comparison of different estimation algorithms [25–31]. Among these, comparison of different kinds of Kalman filters, such as UKF, EKF, and AEKF, is popular [22,26,28]. However, the aforementioned comparative studies either use constant charge/discharge currents or do not consider the impact of temperature on the estimation. Temperature variations are known to introduce a drift in the battery's parameters, which reduces the estimation accuracy. Unlike these studies, the proposed comparative analysis considers both temperature variations and highly nonlinear time-varying charge/discharge current profiles for validation. Design and implementation details of all three estimation algorithms are provided. Experimental results show the accuracy and convergence properties of all estimation methods. The rest of the paper is organized as follows. Section 2 depicts the lithium-ion battery circuit model along with its system dynamics. The proposed strategy of online parameter estimation is detailed in Section 3. Experimental results are reported and discussed in Section 4. A conclusion is drawn based on these results, and future studies in this field are suggested.

2. Modeling of Lithium-Ion Batteries

Similar to other types of batteries, the lithium-ion battery has four main components: positive and negative electrodes, electrolyte, and a separator. Its electric circuit model is shown in Figure 1. The voltage–current characteristic is modeled by an resistance-capacitance (RC) network, with R_b being the internal battery's resistance. On the other side, the OCV–SOC characteristic is represented by a self-discharging resistance, a battery storage capacitor, and a current-controlled current source. To bridge these two networks, a voltage-controlled voltage source is used [32].

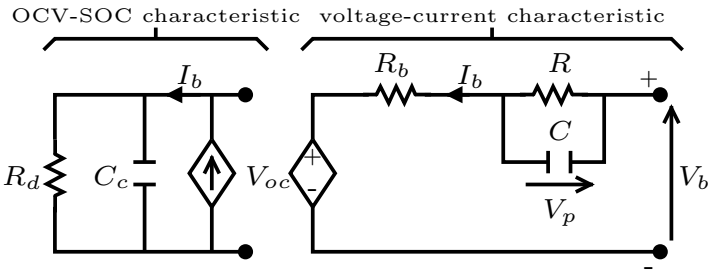

Figure 1. Electric circuit of a lithium battery. OCV: open-circuit voltage; SOC: state of charge.

The voltage–current mathematical model can be represented by the following state equations:

$$\dot{V}_p = \frac{1}{RC} V_p - \frac{1}{C} I_b \tag{1}$$

$$V_b = V_{oc} + V_p + R_b I_b \tag{2}$$

where V_b is the voltage at battery terminals, I_b is the current at battery terminals, V_{oc} is the open circuit voltage, R_b is the internal resistance, R is the equivalent resistance, C is the equivalent capacitance, and V_p is the voltage across the RC network.

In this paper, we aim to estimate the OCV (i.e., V_{oc}), as it is directly related to the battery's SOC by considering the parameters R, C, and R_b as unknown. The battery system's measurable parameters are the battery's terminal voltage V_b and current I_b. The current I_b is assumed as positive in charge mode and negative in discharge. The battery's terminal voltage V_b, current I_b, and their derivatives $\dot{V}_b$, $\dot{I}_b$ are taken to be bounded and continuous in nature. The estimation algorithm sampling frequency is to be high enough such that the variation of the battery's OCV between two samples is negligible (i.e., $\dot{V}_{oc} \approx 0$). Finally, the V_b and I_b are continuously excited.

3. Online Parameter Estimation

In this section, LMS, RLS, and adaptive observer algorithms are designed to estimate the online battery's OCV. Rearranging Equation (2) leads to:

$$V_p = V_b - V_{oc} - R_b I_b$$

Substituting V_p in (1) and considering the aforementioned assumptions gives:

$$\dot{V}_b - \frac{1}{RC} V_b - R_b \dot{I}_b + \frac{R_b}{RC} I_b + \frac{1}{C} I_b + \frac{1}{RC} V_{oc} = 0 \tag{3}$$

Multiplying with RC yields:

$$V_b = RC\dot{V}_b - R_b RC\dot{I}_b + (R + R_b) I_b + V_{oc} \tag{4}$$

Therefore, the battery's dynamics (4) can be expressed using the following regression model:

$$RC\dot{V}_b - R_bRC\dot{I}_b + (R + R_b)I_b + V_{oc} = \Psi^T W \tag{5}$$

where $\Psi \in \mathbb{R}^4 = [\dot{V}_b \ \dot{I}_b \ I_b \ 1]$ is a vector of known functions (regressor), and $W \in \mathbb{R}^4$ is a vector of parameters:

$$\begin{aligned} W_1 &= RC \\ W_2 &= -R_bRC \\ W_3 &= R + R_b \\ W_4 &= V_{oc} \end{aligned} \tag{6}$$

Hence, precise estimation of parameter W_4 eventually leads to an accurate *SOC* estimation. Thus, the output of an adaptive filter can be expressed as:

$$\hat{V}_b = \Psi^T \hat{W} \tag{7}$$

where $\hat{W}$ is the filter's parameter estimate vector. Therefore, the estimation error can be defined as:

$$e_b = V_b - \hat{V}_b \tag{8}$$

To achieve accurate *OCV* estimation, three different algorithms (i.e., *LMS*, *RLS*, and adaptive observer) are designed to drive the estimation error e_b to zero. *LMS* algorithm is a widely used algorithm in adaptive filters, and is known for a low computational complexity. In addition, *RLS* algorithm is another adaptive filter where the coefficients are calculated recursively, which minimizes the weighted linear least squares cost function related to input signals. Unlike the other algorithms, *RLS* input signals are considered as deterministic, whereas in *LMS* they are considered as stochastic. In contrast to the other algorithms, *RLS* converges extremely quickly, but at the cost of higher computational complexity. Similar to *RLS*, adaptive observers offer fast convergence with the simplicity of *LMS* [8]. Moreover, The adaptive observer estimator's stability is guaranteed by Lyapunov's direct method, unlike the aforementioned methods. Next, the proposed methods for the online *OCV* estimation approach are explained.

3.1. Least Mean Square Filter

The *LMS* algorithm emerged as a simple yet effective method for the operation of adaptive finite impulse response (FIR) filters. *LMS*-based algorithms are model-independent because no statistical knowledge about the system in hand is needed in deriving them. Rather, it is a stochastic gradient algorithm that uses simple computational terms to iterate the weights in the direction of the gradient of the squared magnitude of the error signal, as follows:

$$\Delta\hat{W}(k) = \mu\, \Psi(k)\, e_b(k) \tag{9}$$

where k is the discrete-time index and μ is a step-size or adaptation constant rate. Here, the step-size μ influences the filter's coefficients or weights since a large value would lead to high fluctuations in filter weights estimation. On the other hand, if the chosen μ is too small, time taken for convergence to optimal weights would be too long. Therefore, optimal selection of μ is necessary, and a series of tests are usually performed to find a reasonable step-size. However, it is better to have a slower convergence rate and a more accurate output than fluctuating output because of high step-size. Algorithm 1 shows the step-by-step process used by the *LMS* filter.

Algorithm 1 *LMS* filter.

Begin
Step 1: Initialize the vector of parameters $\hat{W}$ to a set of predefined values.
Repeat
Step 2: Compute the battery voltage estimation law in (7).
Step 3: From (8), calculate the estimation error.
Step 4: Compute the vector parameters update using (9).
Step 5: Update the vector parameters using, $\hat{W}(k) = \hat{W}(k-1) + \Delta\hat{W}(k)$.
until Receives the stop request.
End

3.2. Recursive Least Square Filter

The *RLS* algorithm uses the inverse correlation matrix of the input data, leading to a higher performance at the expense of an increase in computational complexity with respect to *LMS*. *RLS*-based algorithms are model-dependent, since their derivatives assume the use of a multivariate Gaussian model. The *RLS* filter recursively computes the filter coefficients update by minimizing a weighted least-squared cost function as follows:

$$\Delta\hat{W}(k) = G(k)\, e_b(k) \tag{10}$$

where $G(k)$ is the gain vector, which is updated as:

$$G(k+1) = \frac{P(k)\Psi(k+1)}{\lambda + \Psi^T(k+1)P(k)\Psi(k+1)} \tag{11}$$

where $P(k)$ is the inverse correlation matrix of the input vector. The standard *RLS* algorithm uses the following equation to update the inverse correlation matrix:

$$P(k+1) = \frac{1}{\lambda}\left(P(k) - \frac{P(k)\Psi(k+1)\Psi(k+1)^T P(k)}{\lambda + \Psi^T(k+1)P(k)\Psi(k+1)}\right) \tag{12}$$

Here, λ is the forgetting factor required as an exponential factor to give less weight to past errors. If $\lambda = 0$, the algorithm has no memory. Conversely, the algorithm has an infinite memory with $\lambda = 1$. Therefore, this factor is usually a constant that lies between 0 and 1 in conventional *RLS* algorithms. Algorithm 2 shows the step-by-step process used by the *RLS* filter.

Algorithm 2 *RLS* filter.

Begin
Step 1: Initialize the vector of parameters $\hat{W}$ to a set of predefined values, assign the initial values to gain vector and inverse correlation matrix.
Repeat
Step 2: Compute the battery voltage estimation law in (7).
Step 3: From (8), calculate the estimation error.
Step 4: Compute the gain vector using (11).
Step 5: Compute the inverse correlation matrix update using (12).
Step 6: Compute the vector parameters update using (10).
Step 7: Update the vector parameters using $\hat{W}(k) = \hat{W}(k-1) + \Delta\hat{W}(k)$.
until Receives the stop request.
End

3.3. Adaptive Observer

Similar to adaptive filters, adaptive observers can also track parameters online as they vary over time. In here, the design and implementation details of an adaptive observer are laid out and explained [8]. The battery's voltage estimation law is defined as:

$$\hat{V}_b = \hat{R}\hat{C}\dot{V}_r - \hat{R}_b\hat{R}\hat{C}\dot{I}_b + (\hat{R} + \hat{R}_b)I_b + \hat{V}_{oc} \tag{13}$$

with:

$$\dot{V}_r = \dot{\hat{V}}_b - K_p e_b - K_i \int e_b \tag{14}$$

where K_p and K_i are the proportional and integral gains, respectively. Substituting (14) into (13) gives:

$$\hat{V}_b = \hat{R}\hat{C}\dot{\hat{V}}_b - \hat{R}\hat{C}K_p e_b - \hat{R}\hat{C}K_i \int e_b - \hat{R}_b\hat{R}\hat{C}\dot{I}_b + (\hat{R} + \hat{R}_b)I_b + \hat{V}_{oc} \tag{15}$$

Adding and subtracting $\hat{R}\hat{C}\dot{V}_b$ on the right side of the above equation gives:

$$\hat{V}_b = -\hat{R}\hat{C}\dot{e}_b - \hat{R}\hat{C}K_p e_b - \hat{R}\hat{C}K_i \int e_b - \hat{R}_b\hat{R}\hat{C}\dot{I}_b + (\hat{R} + \hat{R}_b)I_b + \hat{R}\hat{c}\dot{V}_b + \hat{V}_{oc} \tag{16}$$

Subtracting (5) from (16) and using linear regression gives:

$$\dot{e}_b + (K_p + \hat{\beta})e_b + K_i \int e_b = \hat{\beta}\Psi^T\widetilde{W} \tag{17}$$

where $\widetilde{W} = W - \hat{W}$ and $\beta = (1/RC)$. So, the estimation law (13) gives the closed-loop dynamics as follows:

$$\dot{e}_b + (K_p + \hat{\beta})e_b + K_i \int e_b = 0 \tag{18}$$

The state-space form of the above equation can be written as:

$$\dot{X} = AX + BU \tag{19}$$

where $X \in \mathbb{R}^2 = [\int e_b \; e_b]^T$ is the state vector and $U \in \mathbb{R} = \hat{\beta}\Psi^T\widetilde{W}$ is the state-space input. $A \in \mathbb{R}^{2x2}$ and $B \in \mathbb{R}^2$ are given by:

$$A = \begin{bmatrix} 0 & 1 \\ -K_i & -(K_p + \hat{\beta}) \end{bmatrix}, \; B = \begin{bmatrix} 0 \\ 1 \end{bmatrix}$$

Hence, the estimator's gains K_p and K_i can be chosen to place the closed loop poles at desired places using a pole placement technique. For the given nonlinear system, the adaptive estimator's stability and error's convergence to zero can be guaranteed with the following adaptation law:

$$\dot{\hat{W}} = -\Gamma\Psi B^T P X \tag{20}$$

where $\Gamma = [\gamma_1, \gamma_2]$ and γ_i is a positive constant gain and P is a symmetric positive definite matrix which is chosen to satisfy the Lyapunov equation:

$$A^T P + PA = -Q \tag{21}$$

where Q is a positive definite matrix. Algorithm 3 shows the step-by-step process of the adaptive observer.

Algorithm 3 Adaptive Observer [8].

Begin
Step 1: Initialize the vector of parameters $\hat{W}$ to a set of predefined values, and error e to zero.
Repeat
Step 2: Compute the battery voltage estimation law in (7).
Step 3: From (8), calculate the estimation error.
Step 6: Compute the vector parameters update $\Delta\hat{W}(k) = \hat{W}$; i.e., (20).
Step 7: Update the vector parameters using $\hat{W}(k) = \hat{W}(k-1) + \Delta\hat{W}(k)$.
until Receives the stop request.
End

4. Experimental Results

4.1. Setup

To evaluate the performance of the proposed techniques, a 15 Ah lithium-ion battery was subjected to predefined charge/discharge current profiles at various temperatures (0 °C, 10 °C, 25 °C, and 40 °C). For each charge/discharge cycle, the battery's terminal voltage and current were measured as is illustrated in Figure 2. The collected experimental data at different temperatures was used with a sampling time of 1 s to validate the effectiveness of the adaptive filters. The estimated voltage of each technique is compared against the measured terminal voltage. For a better comparison, the relative *OCV* estimation error of between both *LMS* and *RLS* algorithms is calculated with the following relation:

$$\text{Relative error} = V_{oc}(LMS) - V_{oc}(RLS)$$

In addition, the estimated battery's voltage and *OCV* obtained with the adaptive observer presented in [5] are shown as a benchmark.

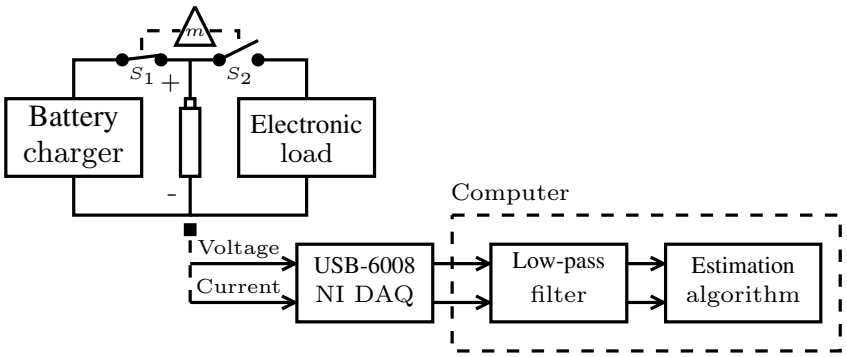

Figure 2. Illustration of the experimental setup.

4.2. Results

The lithium-ion battery was charged using the battery's current profile shown in Figure 3. Experimental results under this condition are depicted in Figures 4–6. As it is shown in Figure 4, both adaptive filters demonstrated a good ability in providing smooth *OCV* estimation at transient and steady-state conditions for different temperatures (0 °C, 10 °C, 25 °C, and 40 °C). As expected, the *RLS* algorithm showed a faster convergence. The battery's voltage estimation (shown in Figure 5) displayed good tracking for all methods. On the other hand, spikes were observed in the battery's voltage due to discontinuous charging current profile (Figure 3). Despite these nonlinearities, the adaptive approaches were able to provide smooth *OCV* estimation (Figure 4). The relative *OCV* estimation error depicted in Figure 6 shows that although *LMS* had a slower convergence compared

to *RLS*, it was able to gradually drive its relative estimation error to *RLS* to zero. Moreover, the initial error for all temperatures was kept in an acceptable range (±0.05 V). It is noteworthy that even if the estimation of parameters requires persistent excitation in several adaptive systems, the fact that *OCV* can be estimated at equilibrium state makes the estimator independent of this requirement.

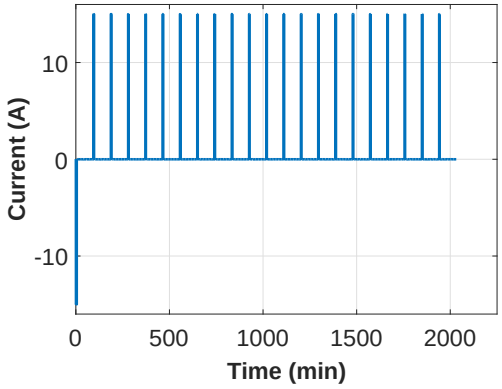

Figure 3. Battery's charge current profile.

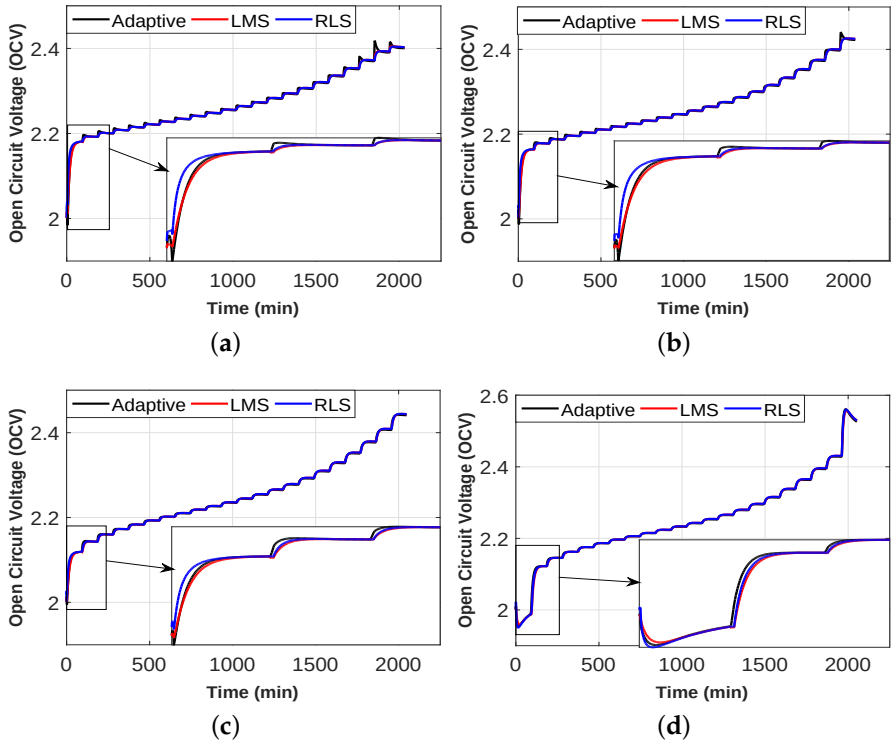

Figure 4. Open circuit voltage (*OCV*) estimation for different temperatures in charge mode. (**a**) 0 °C; (**b**) 10 °C; (**c**) 25 °C; and (**d**) 40 °C. *LMS*: least mean square; and *RLS*: recursive least square.

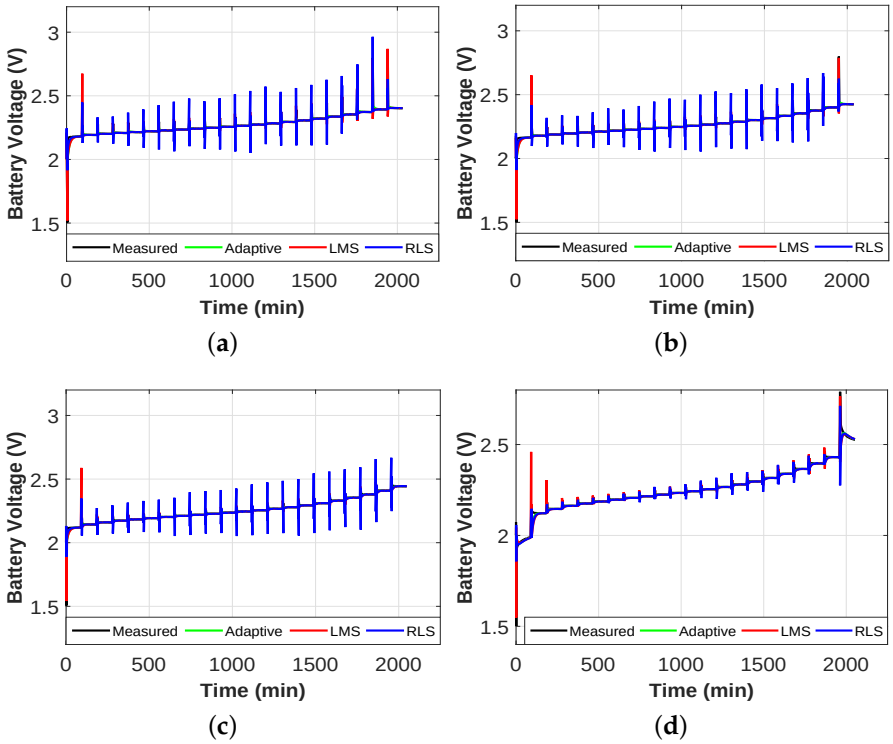

Figure 5. Battery's voltage at different temperatures in charge mode. (**a**) 0 °C; (**b**) 10 °C; (**c**) 25 °C; and (**d**) 40 °C.

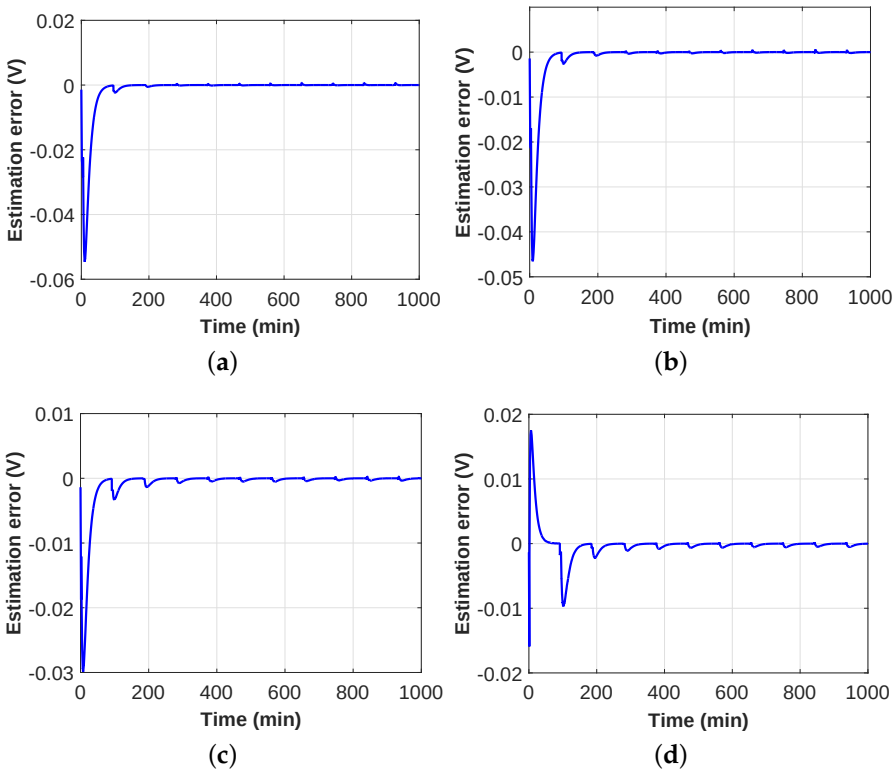

Figure 6. Relative error at different temperatures in charge mode. (**a**) 0 °C; (**b**) 10 °C; (**c**) 25 °C; and (**d**) 40 °C.

Then, the battery was discharged using the current profile shown in Figure 7. Experimental results for discharge mode are illustrated in Figures 8–10. In this case, the deviation of the *OCV* estimates from the expected value was larger, which resulted in higher errors at startup and few oscillations. This was expected, since the other estimated parameters were not yet converged to the expected values. As illustrated in Figure 8, the *OCV* gradually converged to its desired values for all temperatures (0 °C, 10 °C, 25 °C, and 40 ° C). Again, *RLS* showed a faster convergence. In addition, the abrupt change in current again caused spikes in voltage estimation, as shown in Figure 9. The relative error for discharge mode is depicted in Figure 10. Again, smooth error convergence to zero was observed in the presence of current nonlinearities.

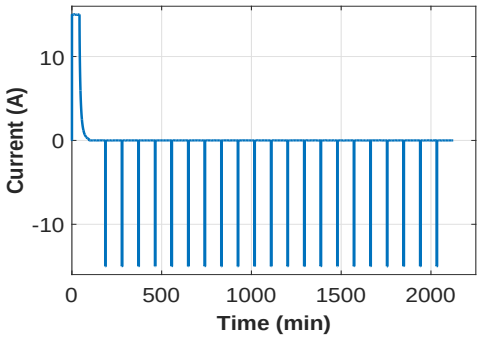

Figure 7. Battery's discharge current profile.

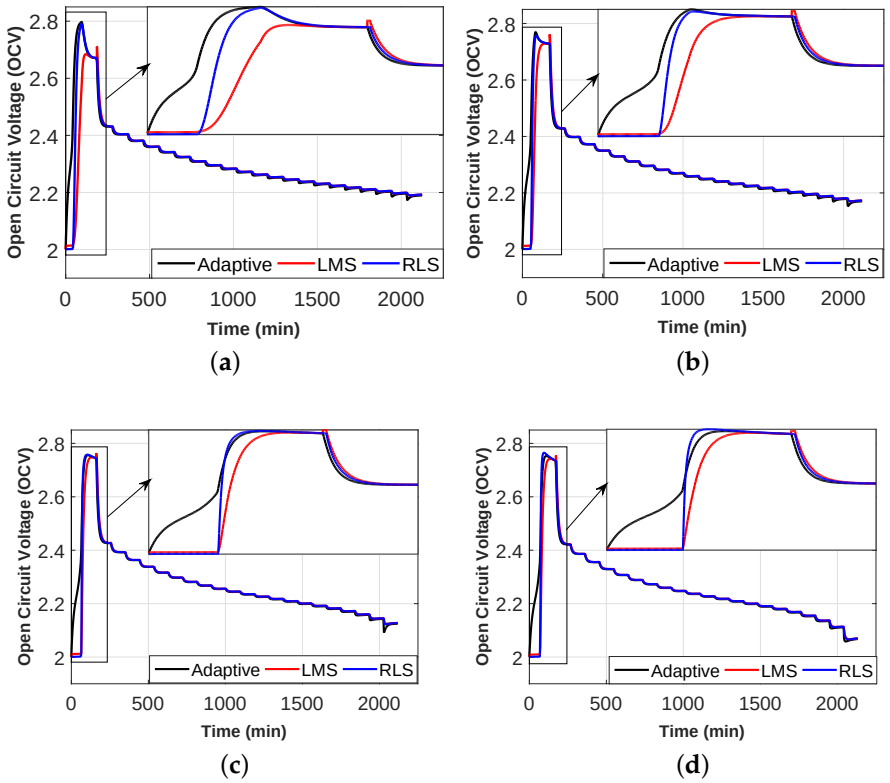

Figure 8. Open-circuit voltage estimation for different temperatures in discharge mode. (**a**) 0 °C; (**b**) 10 °C; (**c**) 25 °C; and (**d**) 40 °C.

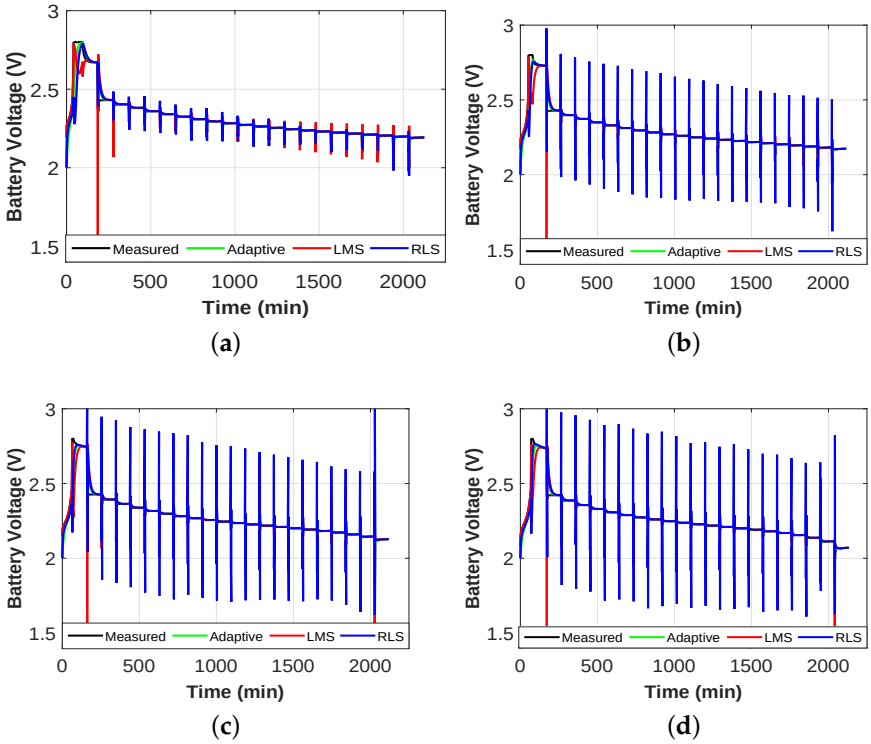

Figure 9. Battery's voltage at different temperatures in discharge mode. (**a**) 0 °C; (**b**) 10 °C; (**c**) 25 °C; and (**d**) 40 °C.

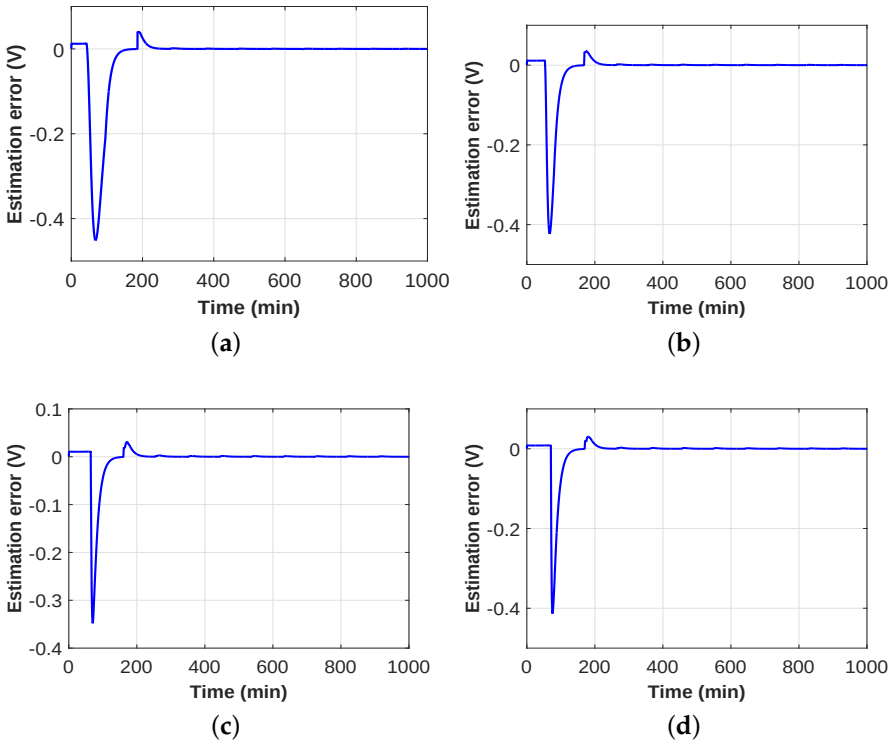

Figure 10. Relative error at different temperatures in discharge mode. (**a**) 0 °C; (**b**) 10 °C; (**c**) 25 °C; and (**d**) 40 °C.

5. Conclusions

In this paper, online *OCV* estimation was achieved for lithium-ion batteries at different temperatures. The proposed strategy makes use of three different algorithms to provide smooth *OCV* estimation using the battery's terminal voltage and current. Experimental results highlight the proposed estimator's performance. Both adaptive filters show high performance in estimating the battery's *OCV* for charge/discharge modes at various temperatures. *RLS* showed a faster convergence, which confirms the credentials for this technique in providing better transient performance at the expense of a higher computation. However, the *LMS* algorithm gradually eliminates the gap, which yields the same estimation as its *RLS* counterpart. Experimental results for an adaptive observer are presented as a benchmark. All methods demonstrate different estimation capabilities at various operating conditions.

Acknowledgments: The authors gratefully acknowledge the financial support for this work from the college of engineering of Tennessee Technological University.

Author Contributions: Both authors have contributed to the preparation of the experimental raw data, programming, and the writing of the paper.

Conflicts of Interest: The authors declare no conflict of interest.

References

1. Kim, M.Y.; Kim, C.H.; Kim, J.H.; Moon, G.W. A chain structure of switched capacitor for improved cell balancing speed of lithium-ion batteries. *IEEE Trans. Ind. Electron.* **2014**, *61*, 3989–3999.
2. Kuperman, A.; Levy, U.; Goren, J.; Zafransky, A.; Savernin, A. Battery charger for electric vehicle traction battery switch station. *IEEE Trans. Ind. Electron.* **2013**, *60*, 5391–5399.
3. Ranjbar, A.H.; Banaei, A.; Khoobroo, A.; Fahimi, B. Online estimation of state of charge in li-ion batteries using impulse response concept. *IEEE Trans. Smart Grid* **2012**, *3*, 360–367.
4. He, H.; Xiong, R.; Zhang, F.S.; Fan, J. State-of-charge estimation of the lithium-ion battery using an adaptive extended Kalman filter based on an improved Thevenin model. *IEEE Trans. Veh. Technol.* **2011**, *60*, 1461–1469.
5. Chaoui, H.; Golbon, N.; Hmouz, I.; Souissi, R.; Tahar, S. Lyapunov-based adaptive state of charge and state of health estimation for lithium-ion batteries. *IEEE Trans. Ind. Electron.* **2015**, *62*, 1610–1618.
6. Kim, I.S. Nonlinear state of charge estimator for hybrid electric vehicle Battery. *IEEE Trans. Power Electron.* **2008**, *23*, 2027–2034.
7. Chaoui, H.; Sicard, P. Accurate state of charge (SOC) estimation for batteries using a reduced-order observer. In Proceedings of the 2011 IEEE International Conference on Industrial Technology, Taipei, Taiwan, 14–16 March 2011; pp. 39–43.
8. Chaoui, H.; Gualous, H. Adaptive state of charge estimation of lithium-ion batteries with parameter and thermal uncertainties. *IEEE Trans. Control Syst. Technol.* **2016**, *25*, 752–759.
9. Partovibakhsh, M.; Liu, G. An adaptive unscented Kalman filtering approach for online estimation of model parameters and state-of-charge of lithium-ion batteries for autonomous mobile robots. *IEEE Trans. Control Syst. Technol.* **2014**, *23*, 357–363.
10. Chen, Z.; Fu, Y.; Mi, C.C. State of charge estimation of lithium-ion batteries in electric drive vehicles using extended Kalman filtering. *IEEE Trans. Veh. Technol.* **2013**, *62*, 1020–1030.
11. Chen, X.; Shen, W.; Dai, M.; Cao, Z.; Jin, J.; Kapoor, A. Robust adaptive sliding-mode observer using RBF neural network for lithium-ion battery state of charge estimation in electric vehicles. *IEEE Trans. Veh. Technol.* **2016**, *65*, 1936–1947.
12. Paschero, M.; Storti, G.L.; Rizzi, A.; Mascioli, F.M.F.; Rizzoni, G. A novel mechanical analogy-based battery model for SoC estimation using a Multicell EKF. *IEEE Trans. Sustain. Energy* **2016**, *7*, 1695–1702.
13. Luzi, M.; Paschero, M.; Rossini, A.; Rizzi, A.; Mascioli, F.M.F. Comparison between two nonlinear Kalman Filters for reliable SoC estimation on a prototypal BMS. In Proceedings of the 42nd Annual Conference of the IEEE Industrial Electronics Society, IECON, Florence, Italy, 23–26 October 2016; pp. 5501–5506.
14. Zhang, Z.L.; Cheng, X.; Lu, Z.Y.; Gu, D.J. SOC estimation of lithium-ion batteries with AEKF and wavelet transform matrix. *IEEE Trans. Power Electron.* **2016**, *PP*, doi:10.1109/TPEL.2016.2636180.

15. Ma, Y.; Zhou, X.; Li, B.; Chen, H. Fractional modeling and SOC estimation of lithium-ion battery. *IEEE/CAA J. Autom. Sin.* **2016**, *3*, 281–287.
16. Zhang, F.; Liu, G.; Fang, L.; Wang, H. Estimation of battery state of charge with H_∞ observer: Applied to a robot for inspecting power transmission lines. *IEEE Trans. Ind. Electron.* **2011**, *59*, 1086–1095.
17. Lee, Y.-S.; Wang, W.Y.; Kuo, T.Y. Soft computing for battery state-of-charge (BSOC) estimation in battery string systems. *IEEE Trans. Ind. Electron.* **2008**, *55*, 229–239.
18. Charkhgard, M.; Farrokhi, M. State-of-charge estimation for lithium-ion batteries using neural networks and EKF. *IEEE Trans. Ind. Electron.* **2010**, *57*, 4178–4187.
19. Lin, H.-T.; Liang, T.J.; Chen, S.M. Estimation of battery state of health using probabilistic neural network. *IEEE Trans. Ind. Inf.* **2013**, *9*, 679–685.
20. Li, I.-H.; Wang, W.-Y.; Su, S.-F.; Lee, Y.S. A merged fuzzy neural network and its applications in battery state-of-charge estimation. *IEEE Trans. Energy Convers.* **2007**, *22*, 697–708.
21. Lin, F.-J.; Huang, M.-S.; Yeh, P.-Y.; Tsai, H.C.; Kuan, C.H. DSP-based probabilistic fuzzy neural network control for Li-ion battery charger. *IEEE Trans. Power Electron.* **2012**, *27*, 3782–3794.
22. Zhang, Y.; Xiong, R.; He, H. Evaluation of the model-based state-of-charge estimation methods for lithium-ion batteries. In Proceedings of the 2016 IEEE Transportation Electrification Conference and Expo (ITEC), Dearborn, MI, USA, 27–29 June 2016; pp. 1–8.
23. Koirala, N.; He, F.; Shen, W. Comparison of two battery equivalent circuit models for state of charge estimation in electric vehicles. In Proceedings of the 2015 IEEE 10th Conference on Industrial Electronics and Applications (ICIEA), Auckland, New Zealand, 15–17 June 2015; pp. 17–22.
24. Liu, G.; Lu, L.; Fu, H.; Hua, J.; Li, J.; Ouyang, M.; Wang, Y.; Xue, S.; Chen, P. A comparative study of equivalent circuit models and enhanced equivalent circuit models of lithium-ion batteries with different model structures. In Proceedings of the 2014 IEEE Conference and Expo Transportation Electrification Asia-Pacific (ITEC Asia-Pacific), Beijing, China, 31 August–3 September 2014; pp. 1–6.
25. Berrueta, A.; Martín, I.S.; Sanchis, P.; Ursúa, A. Comparison of State-of-Charge estimation methods for stationary Lithium-ion batteries. In Proceedings of the 42nd Annual Conference of the IEEE Industrial Electronics Society, IECON, Florence, Italy, 23–26 October 2016; pp. 2010–2015.
26. Farag, M.S.; Ahmed, R.; Gadsden, S.A.; Habibi, S.R.; Tjong, J. A comparative study of Li-ion battery models and nonlinear dual estimation strategies. In Proceedings of the 2012 IEEE Transportation Electrification Conference and Expo (ITEC), Dearborn, MI, USA, 18–20 June 2012; pp. 1–8.
27. Xu, J.; Cao, B.; Cao, J.; Zou, Z.; Mi, C.C.; Chen, Z. A comparison study of the model based SOC estimation methods for lithium-ion batteries. In Proceedings of the 2013 IEEE Vehicle Power and Propulsion Conference (VPPC), Beijing, China, 15–18 October 2013; pp. 1–5.
28. Meng, J.; Luo, G.; Gao, F. State-of-charge estimation for lithium-ion battery using AUKF and LSSVM. In Proceedings of the 2014 IEEE Conference and Expo Transportation Electrification Asia-Pacific (ITEC Asia-Pacific), Beijing, China, 31 August–3 September 2014; pp. 1–6.
29. Lagraoui, M.; Doubabi, S.; Rachid, A. SOC estimation of Lithium-ion battery using Kalman filter and Luenberger observer: A comparative study. In Proceedings of the 2014 International Renewable and Sustainable Energy Conference (IRSEC), Ouarzazate, Morocco, 17–19 October 2014; pp. 636–641.
30. Chen, X.; Shen, W.; Cao, Z.; Kapoor, A. A comparative study of observer design techniques for state of charge estimation in electric vehicles. In Proceedings of the 2012 7th IEEE Conference on Industrial Electronics and Applications (ICIEA), Singapore, 18–20 July 2012; pp. 102–107.
31. Jian, W.; Jiang, X.; Zhang, J.; Xiang, Z.; Jian, Y. Comparison of SOC estimation performance with different training functions using neural network. In Proceedings of the 2012 UKSim 14th International Conference on Computer Modelling and Simulation, Cambridge, UK, 28–30 March 2012; pp. 459–463.
32. Chen, M.; Rincon-Mora, G.A. Accurate electrical battery model capable of predicting runtime and I-V performance. *IEEE Trans. Energy Convers.* **2006**, *21*, 504–511.